

Enhanced visible-light photo-oxidation of nitric oxide using bismuth-coupled graphitic carbon nitride composite heterostructures

Yuhan LI^a, Kangle LV^{a,c,*}, Wing-Kei HO^{a,b,*}, Zaiwang ZHAO^a, Huang YU^b

^aDepartment of Science and Environmental Studies, The Education University of Hong Kong, Tai Po, N.T., Hong Kong, China

^bKey Laboratory of Aerosol Chemistry and Physics, Institute of Earth Environment, Chinese Academy of Sciences, Xi'an 710061, Shanxi, China

^cKey Laboratory of Catalysis and Materials Science of the State Ethnic Affairs Commission and Ministry of Education, College of Resources and Environmental Science, South-Central University for Nationalities, Wuhan 430074, Hubei, China

Abstract

Pure bismuth (Bi) metal-modified graphitic carbon nitride (g-C₃N₄) composites (Bi-CN) with a pomegranate-like structure were prepared by an *in situ* method. The Bi-CN composites were used as photocatalysts for the oxidation of nitric oxide (NO) under visible-light irradiation. The inclusion of pure Bi metal in the g-C₃N₄ layers markedly improved the light absorption of the Bi-CN composites from the ultraviolet to the near-infrared region because of the typical surface plasmon resonance of Bi metal. The separation and transfer of photogenerated charge carriers were greatly accelerated by the presence of built-in Mott–Schottky effects at the interface between Bi metal and g-C₃N₄. As a result, the Bi-CN composite photocatalysts exhibited considerably enhanced efficiency in the photocatalytic removal of NO compared with that of Bi metal or g-C₃N₄ alone. The pomegranate-like structure of the Bi-CN composites and an explanation for their improved photocatalytic activity were proposed. This work not only provides a design for highly efficient g-C₃N₄-based photocatalysts through modification with Bi metal, but also offers new insights into the mechanistic understanding of g-C₃N₄-based photocatalysis.

Keywords: Bismuth; Surface plasmon resonance; Photo-oxidation; Nitric oxide; Visible light; Graphitic carbon nitride

Received 29 August 2016. Accepted 5 October 2016

*Corresponding author. Tel.: +852-2948 8255; Fax: +852-2948 7726; E-mail: lvkangle@mail.scuec.edu.cn (K. L. Lv).

*Corresponding author. E-mail: keithho@ied.edu.hk (W. K. Ho)

1. Introduction

The potential for noble metal-based materials to harvest and convert solar energy has garnered considerable attention in recent years [1–3]. In particular, the ability of noble metals to strongly absorb visible light because of their localized surface plasmon resonance (SPR), which considerably increases their utilization efficiency of visible light, is important for their application [4, 5]. In view of expense of precious metals, some affordable and readily available metals possessing similar

electronic and light-absorption characteristics to those of noble metals have been investigated as substitutes [6–10]. It is well documented that the semimetal bismuth (Bi) behaves as a photocatalyst with promising photocatalytic performance [10]. Pure Bi metal can exhibit admirable photocatalytic reactivity under ultraviolet (UV) irradiation ($\lambda \leq 280$ nm), but its response to visible light is poor [11]. Thus, it is important to develop feasible and environmentally benign strategies to afford Bi with visible-light activity.

Graphitic carbon nitride (g-C₃N₄) can photocatalytically break down various pollutants into harmless chemicals and photocatalyze water conversion to hydrogen and hydrogen peroxide under visible-light irradiation [12–15]. However, the photocatalytic efficiency of bulk g-C₃N₄ is quite low because of its marginal absorption of visible light and poor separation of photogenerated carriers; therefore, effective modification methods need to be developed to improve its visible-light performance. For this reason, a number of g-C₃N₄-based heterostructures with synergetic coupling effects between g-C₃N₄ and other functional materials have been developed to greatly enhance its absorption of visible light and facilitate charge transfer [16–18]. Recently, Dong et al. [19] synthesized Bi nanosphere-modified g-C₃N₄ nanosheets (Bi-g-C₃N₄) with excellent photocatalytic performance. The as-obtained Bi-g-C₃N₄ composites combined with some bismuth oxide (Bi₂O₃) layers offered two major advantages over pure g-C₃N₄ in photocatalytic reactions. On one hand, by loading Bi metal on the surface of g-C₃N₄, Bi-coupled g-C₃N₄ nanocomposites with a strong visible-light response were obtained because of the SPR effects of Bi. On the other hand, the supporting Bi nanospheres accelerated the separation of photogenerated charge carriers because of the formation of a Mott–Schottky barrier at the Bi/g-C₃N₄ interface. However, Bi₂O₃ formed on the surface of Bi-g-C₃N₄ composites can have a shielding effect that deteriorates the above-mentioned contributions from Bi. Dong and colleagues [19] used bismuth nitrate pentahydrate (Bi(NO₃)₃·5H₂O) as the precursor for Bi metal, but the oxidizing ability endowed by NO₃[−] led to the generation of Bi₂O₃ in the resultant composites. Along this line of thinking, it is necessary to prepare pure Bi metal-coupled g-C₃N₄ composites without Bi₂O₃ layers by using a substitute for Bi(NO₃)₃·5H₂O.

Nitric oxide (NO) and nitrogen dioxide (NO₂), jointly referred to as NO_x, are typical indoor and outdoor air pollutants that are causing increasing environmental concern. NO_x is one of the major contributors to acid rain and urban smog, and could result in serious respiratory diseases, hospitalization for heart or lung diseases, and even premature death [19].

In the present study, pure Bi metal-modified g-C₃N₄ (Bi-CN) composites are fabricated by an in situ grafting treatment. These composites show high reactivity in photo-oxidation of NO under visible-light illumination. Sodium bismuthate (NaBiO₃·2H₂O) is successfully used as a precursor of Bi metal to obtain pure Bi metal in the Bi-CN composites. The composites are investigated by X-ray diffraction (XRD), Fourier transform infrared (FT-IR) spectroscopy, and X-ray photoelectron spectroscopy (XPS). The photo-oxidation of NO by the Bi-CN composites is evaluated.

2. Experimental

2.1. Preparation of Bi-CN composites

All chemicals were of analytical grade and used without further purification. We synthesized g-C₃N₄ by heating dicyanamide (20 g) at 550 °C for 2 h. To synthesize the Bi-CN composite photocatalysts, NaBiO₃·2H₂O (0.339 g) was completely dissolved in ethylene glycol (EG, 30 mL) under continuous magnetic stirring and then polyvinylpyrrolidone (PVP, MW 130,000, 0.2 g) was added. The molar ratio of Bi to the repeating unit of PVP was controlled at 1:1.6. A certain amount of g-C₃N₄ was then added to the solution under vigorous stirring. After stirring for 1 h, the mixture was transferred into a 100-mL Teflon-sealed autoclave, sealed and heated at 200 °C for 24 h in a furnace, before cooling to room temperature. The product was centrifuged, and then washed with acetone followed by ethanol several times to remove residual EG and PVP. Bi-CN photocatalysts with different weight ratios of metallic Bi to CN (namely, 5% Bi-CN, 10% Bi-CN, 15% Bi-CN, 25% Bi-CN, and 50% Bi-CN) were synthesized. Metallic Bi and solvothermally prepared g-C₃N₄ (CN-EG) were also prepared as reference samples, using the same procedure as that for the Bi-CN composites except that only either g-C₃N₄ or Bi was added.

2.2. Characterization

The phase structures of the samples were investigated by XRD (D/max RA, Japan). The morphological characteristics and microstructures of the samples were characterized with a scanning electron microscope (SEM; JEOL JSM-6490, Japan). Nitrogen adsorption–desorption isotherms were obtained using a nitrogen adsorption apparatus (ASAP 2020, USA), in which all of the samples were degassed at 150 °C prior to the measurements to investigate their surface areas and pore size distributions. Samples embedded in KBr pellets were subjected to FT-IR spectroscopy in a Nicolet Nexus spectrometer to detect the functional groups on their surfaces. The surface chemical composition and total density of state distribution in the valence band (VB) of each sample were probed using an X-ray photoelectron spectrometer (Thermo ESCALAB 250, USA) with Al K_α X-rays ($h\nu = 1486.6$ eV) operated at 150 W. The shift of the binding energy attributed to relative surface charging was corrected using the C 1s level at 284.8 eV as an internal standard. The optical properties of the samples were measured by an ultraviolet-visible diffuse reflectance spectrophotometer (UV-Vis DRS; UV-2450, Shimadzu, Japan) equipped with an integrating sphere assembly; BaSO₄ was used as the reflectance sample. Photoluminescence (PL) spectra of the samples were obtained with a fluorescence spectrophotometer (FS-2500, Japan) using a Xe lamp with an optical filter as the excitation source to investigate the recombination and separation of photogenerated electrons and holes.

2.3. Visible-light photocatalytic activity.

The photocatalytic activity of the samples was evaluated through the oxidation of NO at the 10⁻⁶ level in a continuous-flow reactor at ambient temperature. The volume of the rectangular reactor composed of stainless steel and covered with quartz glass was 4.5 L (30 × 15 × 10 cm). An LED lamp (448 nm) was used as a simulated visible-light source. Photocatalyst (0.2 g) was added to H₂O (30 mL) and ultrasonicated for 30 min. The resulting suspension was coated onto a dish with a diameter

of 11.5 cm. The coated dish was pretreated at 70 °C to evaporate water thoroughly and then cooled to room temperature prior to photocatalytic testing. NO gas was introduced from a compressed gas cylinder containing 50×10^{-6} NO (balance N₂) in accordance with the traceable standard recommended by the National Institute of Standards and Technology. The initial NO concentration was diluted to approximately 600×10^{-9} by an air stream supplied by a zero-air generator (Advanced Pollution Instrumentation, Teledyne Technologies, Model 701). The gas streams were completely premixed in a gas blender, and the flow rate was controlled at 1.0 L·min⁻¹ with a mass flow controller. After adsorption–desorption equilibrium was achieved, the lamp was turned on. The NO and NO₂ concentrations were continuously measured using a chemiluminescence NO_x analyzer (Advanced Pollution Instrumentation, Teledyne Technologies, Model T200) that monitored NO, NO₂, and NO_x (NO_x represents NO + NO₂) at a sampling rate of 1.0 L·min⁻¹. The removal ratio of NO (η) was calculated as η (%) = $(1 - C/C_0) \times 100\%$, where C and C_0 are the NO concentration in the outlet steam and feed stream, respectively.

3. Results and discussion

3.1. Photocatalytic removal of NO

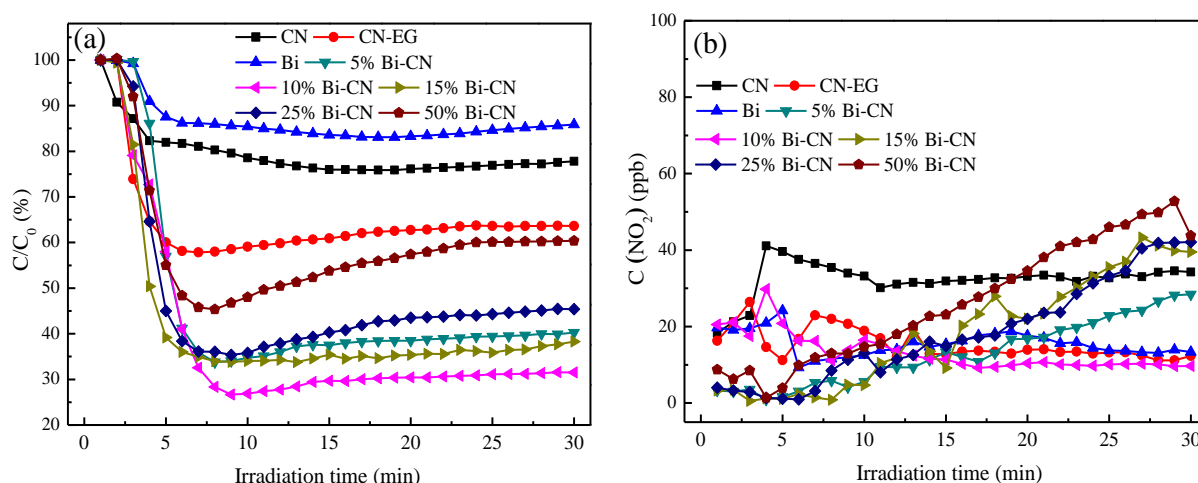


Fig. 1. Photocatalytic removal of NO (a) and monitoring concentration of NO₂ intermediates in a single-pass flow of air over the as-obtained samples under visible-light irradiation (b) (continuous reactor; initial NO concentration: 600×10^{-9}).

The variations of NO removal rate and NO₂ concentration with visible-light irradiation time in the presence of different samples are shown in Fig. 1. Control experiments in the absence of either photocatalyst or light irradiation were also performed, which demonstrated that the presence of both photocatalyst and visible light was required for removal of NO to occur. Fig. 1(a) clearly shows that g-C₃N₄ alone possessed feeble NO photo-oxidation capability, much lower than that of the solvothermally prepared CN-EG, which showed a reasonable η in NO oxidation of approximately 37%. This result showed that EG-assisted solvothermal treatment contributed to the increase of photocatalytic activity of g-C₃N₄ in NO oxidation, as reported in the literature, because of the positive directing effect of EG on the morphology of g-C₃N₄ [20]. In this context, to afford markedly enhanced visible-light activity, various contents of elemental Bi were introduced into the g-C₃N₄-based photocatalyst system. Under visible-light illumination, metallic Bi showed little photocatalytic oxidation NO

activity, likely because Bi alone requires UV irradiation to catalyze NO photo-oxidation [11]. In contrast, the Bi-CN composites displayed much improved photocatalytic oxidation abilities in this process. That these Bi-CN composites exhibited marked enhancement of photocatalytic activity in photo-oxidation of NO compared with both g-C₃N₄ and Bi alone was anticipated. This is because introduction of elemental Bi commonly results in considerable photo-oxidation activity towards NO, which can mainly be attributed to the synergistic effects of improved charge separation and SPR endowed by Bi metal upon irradiation with visible light ($\lambda > 448$ nm) [19]. Nevertheless, Fig. 1(a) reveals that the photo-oxidation reactivities of the Bi-CN composites for NO decreased with increasing Bi metal content beyond the optimum composition of 10% Bi-CN. Excess Bi metal ($> 10\%$) in the Bi-CN composites resulted in a negative influence on the photo-oxidation performance, which could be explained as follows: (1) a large amount of Bi metal on the surface of the Bi-CN composite may physically block g-C₃N₄ from absorbing visible light to the detriment of visible-light-harvesting ability; (2) a substantial content of Bi metal in the Bi-CN composites may strongly absorb UV light ($\lambda < 280$ nm) rather than visible light, thus deteriorating the visible-light-driven photocatalytic oxidation efficiency of the catalyst towards NO.

Fig. 1(a) also shows that several of the photocatalytic oxidation profiles first decreased and then increased with irradiation time. This is because some of the oxidation intermediates and/or products formed during NO oxidation, such as NO₃⁻, were adsorbed on the photocatalyst surface, decreasing the number of active sites and slowing NO degradation [23].

More importantly, as shown in Fig. 1, η (70.4%) and the NO₂ concentration (less than 10×10^{-9}) of 10% Bi-CN are much higher and lower under visible-light irradiation, respectively, than those of reported photocatalytic materials based on modified g-C₃N₄ [21], K-intercalated g-C₃N₄ [22], Ag-doped g-C₃N₄ [23], and even a Bi sphere/g-C₃N₄ nanohybrid with Bi₂O₃ layers [19] (Table 1). This result suggests that a composite consisting of pure Bi metal hybridized with g-C₃N₄ can far outperform those consisting of g-C₃N₄ modified with noble metals, graphene materials, Bi metal with impurities in nitrate formation, displaying both high photo-oxidation ability and selectivity. Therefore, it is worth comprehensively investigating the Bi-CN composite system in terms of structure and physical merits.

Table 1

Physical properties and removal rate of NO for photocatalysts and reference samples.

Sample	A_{BET} (m ² ·g ⁻¹)	V_{pore} (cm ³ ·g ⁻¹)	Peak pore size (nm)	η^a (%)	Ref.
CN	9	0.055	1.8/16.4	22.2	this work
CN-EG	53	0.18	1.8/4.8	36.4	this work
Bi	3	0.026	15.5	14.1	this work
10% Bi-CN	42	0.17	1.9/6.8	70.4	this work
15% Bi-CN	42	0.18	1.8/11.6	61.7	this work

CN-GO	—	—	—	60.7	[21] ^b
K-intercalated g-C ₃ N ₄	—	—	—	36.8	[22] ^c
Ag-doped g-C ₃ N ₄	—	—	—	54.3	[23] ^d
Bi-CN-25	—	—	—	60.2	[19] ^e

^a NO removal ratio.

^b Weight ratio of graphene oxide to mesoporous g-C₃N₄ was controlled at 1.0 wt%.

^c Weight ratio of K to g-C₃N₄ was 5%.

^d Molar ratio of Ag to g-C₃N₄ was 10%.

^e Mass ratio of Bi to g-C₃N₄ was 25%.

The initial NO concentration in the feed gas was 600×10^{-9} and the concentration of NO₂ from the outlet was less than 50×10^{-9} at more than 50% NO conversion (Fig. 1(a) and (b)), indicating that NO₂ was not the major product. This is because NO₂ is not the final product of NO photo-oxidation; NO₂ can further oxidize to NO₃⁻ over g-C₃N₄ [23]. However, quantitative detection of the NO oxidation intermediates adsorbed on the photocatalyst surface still remains a great challenge.

3.2. Photocatalyst structure and composition

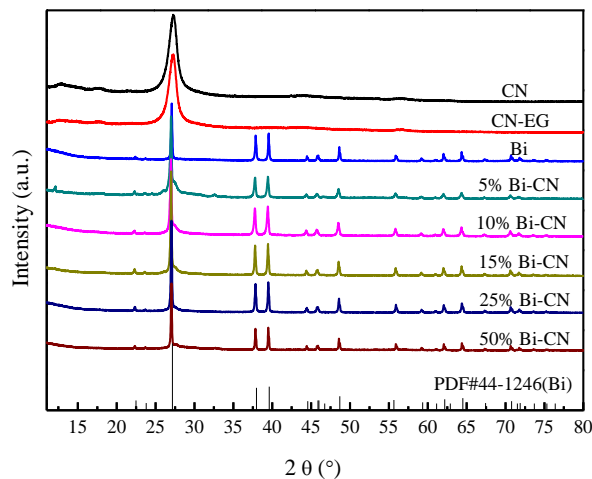


Fig. 2. XRD patterns of the photocatalytic materials.

To ascertain whether or not Bi exists in the Bi-CN composites in its elemental form, XRD was carried out. Fig. 2 reveals that the pattern of CN-EG is quite similar to that of pristine g-C₃N₄. However, CN-EG showed a slightly broadened main peak centered at around 27.5° compared with that of g-C₃N₄, which may result from the decreased crystallite size following solvothermal treatment. The XRD patterns of the Bi-CN composites contained peaks consistent with the rhombohedral phase of Bi metal (JCPDS PDF card 44-1246), which confirmed the existence of Bi metal in the Bi-CN composites. No obvious diffraction peaks of g-C₃N₄ could be discerned because of the strong shadowing effect of the (012) peak of the Bi metal phase in the Bi-CN composites [19]. The presence of g-C₃N₄ in the Bi-CN composites was verified by FT-IR and XPS

analyses.

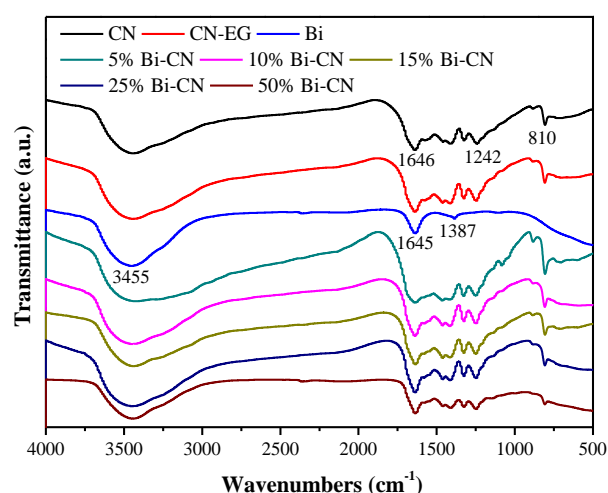
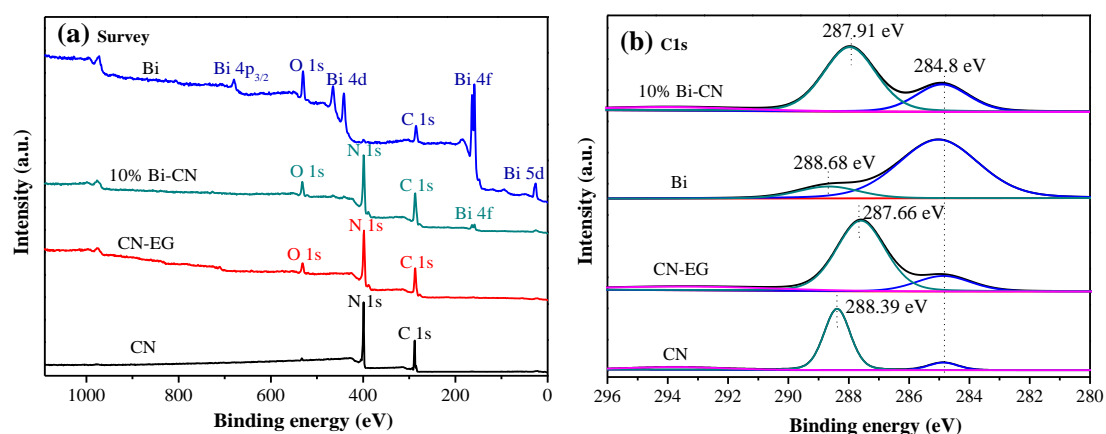


Fig. 3. FT-IR spectra of g-C₃N₄ (CN), CN-EG, Bi, and Bi-CN composites.

The chemical bonding of the bare g-C₃N₄, CN-EG, Bi, and Bi-CN composites was investigated by FT-IR spectroscopy. The solvothermally prepared CN-EG displayed FT-IR features akin to those of the pristine g-C₃N₄ (Fig. 3). Peaks observed at approximately 810 and 1242–1646 cm⁻¹ were attributed to the characteristic breathing mode of a triazine ring system and typical stretching vibration modes of a g-C₃N₄ heterocycle, respectively. Two strong bands centered at 1387 and 1645 cm⁻¹ were consistent with the presence of Bi metal [24]. All of the main characteristic peaks of g-C₃N₄ and pure Bi were observed in the FT-IR spectra of all the Bi-CN composites, confirming the formation of composites between elemental Bi and g-C₃N₄ by solvothermal treatment. These Bi-CN composites may offer electron migration routes to improve photoinduced charge carrier separation and enhance photoactivity.



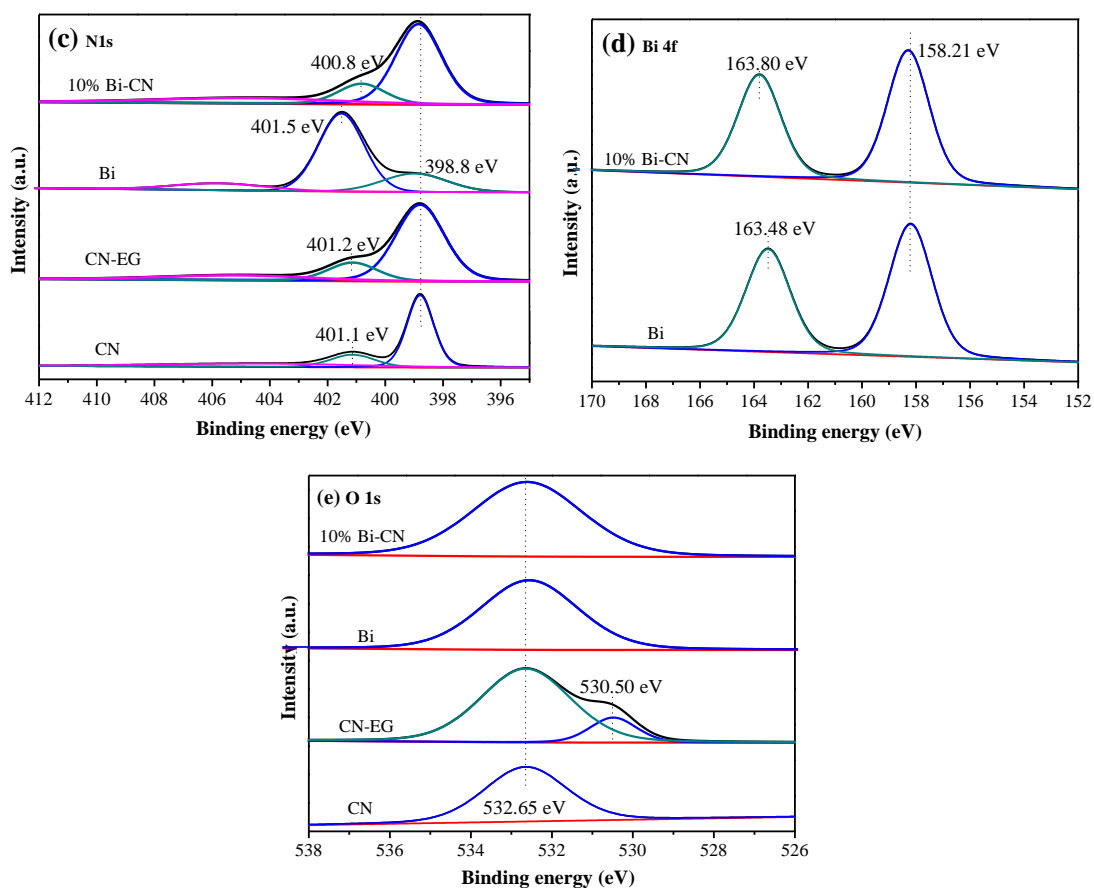


Fig. 4. XPS analysis of g-C₃N₄ (CN), CN-EG, Bi, and 10% Bi-CN composites. (a) Survey scan; (b) C 1s; (c) N 1s; (d) Bi 4f; and (e) O 1s.

XPS analysis was conducted to investigate the surface chemical composition of the Bi-CN composites and the chemical state of Bi in them. The survey spectra in Fig. 4(a) reveal that g-C₃N₄ and CN-EG were composed of C, N, and a small amount of O originating from contamination from the atmosphere; no other peaks were observed. The spectrum for elemental Bi indicated the presence of Bi, C, and O species; the latter two may result from the easy oxidation of adventitious carbon species in the air. The 10% Bi-CN composite contained Bi, C, N, and a small amount of O, which could originate from the surface absorption of g-C₃N₄. This spectrum indicates that the Bi in the 10% Bi-CN composite existed in its elemental form.

The high-resolution C 1s spectra in Fig. 4(b) can be deconvoluted into two dominant peaks with binding energies of ~284.8 and ~288.39 eV. The peak located at 284.8 eV may be related to C–C and/or adventitious carbon, and that at 288.39 eV can be assigned to the N–C–N group of g-C₃N₄. The high-resolution N 1s spectra in Fig. 4(c) could be fitted into two predominant peaks at 398.8 and 401.1 eV and a weak peak at 404.5 eV, which are ascribed to C=N–C, C–N–H, and π -excitation, respectively. According to the C 1s and N 1s results, the composites contain no functional groups related to Bi–C or Bi–N, indicating that elemental Bi was the major phase on the surface of the Bi-CN composites. The XPS data for Bi in Fig. 4(d) provide further evidence for the existence of elemental Bi in the Bi-CN composites. The Bi 4f spectra could

be fitted into a doublet corresponding to metallic Bi $4f_{7/2}$ and metallic Bi $4f_{5/2}$ at binding energies of 158.21 and 163.48 eV, respectively, which are almost equal to the standard binding energy of pure Bi metal. Furthermore, no other impurity phase was detected, such as the presence of Bi–O bonds. This revealed the presence of pure Bi metal in the 10% Bi-CN composite without any oxide impurities. Therefore, the 10% Bi-CN composite can take full advantage of the SPR effects derived from pure Bi metal to enhance its photocatalytic performance.

The O 1s spectrum (Fig. 4(e)) was fitted into one peak at a binding energy of 532.65 eV, which was ascribed to adsorbed H₂O. As reported previously, the introduction of amine groups into a carbon carrier can result in an increased percentage of zeroth-order metal that is resistant to re-oxidation during air contact [25]. In our Bi-CN composite system, the solvothermally prepared g-C₃N₄ has a high nitrogen content. These π -bonded planar C–N–C layers along with their incompletely condensed amino groups can stabilize highly dispersed Bi and prevent its oxidation. Additionally, the use of NaBiO₃·2H₂O as a precursor avoids the oxidation of Bi metal during the composite preparation process.

3.3. Optical properties and possible photocatalytic mechanism

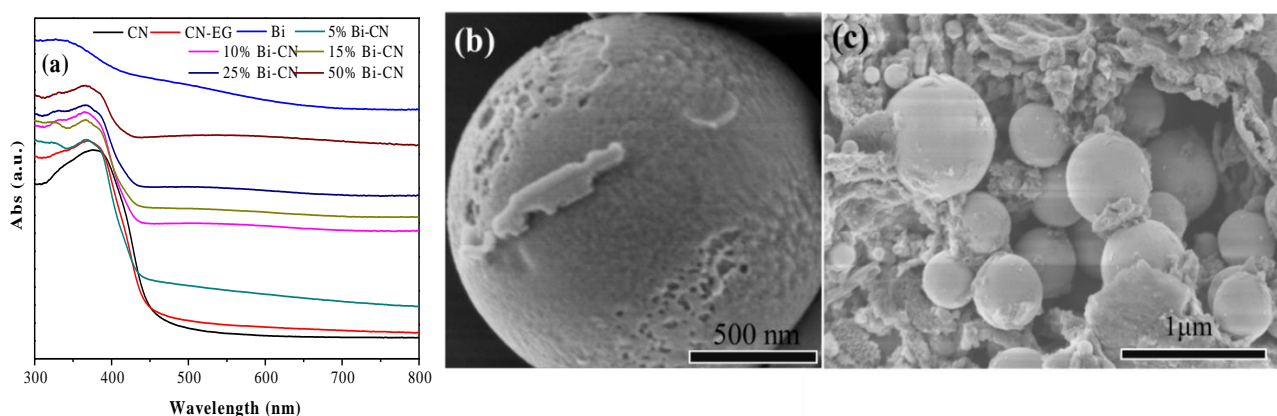


Fig. 5. UV-vis DRS of g-C₃N₄ (CN), CN-EG, Bi, and Bi-CN composites (a). SEM images of Bi (b) and 10% Bi-CN composite (c).

To explore the underlying photocatalytic mechanism of the composites, their optical properties were investigated by UV-vis DRS; the results are illustrated in Fig. 5. The absorption band edges of both g-C₃N₄ and CN-EG appeared at $\lambda < 465$ nm, which were attributed to the distinctive absorption of g-C₃N₄ with a band-gap energy of ca. 2.7 eV. In contrast, the Bi-CN composites strongly absorbed light from the UV to the near-infrared range (200–800 nm) after the introduction of Bi. The absorption intensity of the Bi-CN composites gradually strengthened with increasing Bi content, which in turn increased the utilized efficiency of solar light, and thus improved photocatalytic oxidation capacity. The strong light absorption of the Bi-CN composites originated from the characteristic SPR effect of Bi metal. Dong et al. [19] reported that pure Bi nanoparticles with diameters of 150–200 nm displayed a SPR peak centered at approximately 500 nm. However, in our case, no peaks characteristic of the SPR of Bi metal were observed in the range of 200–800 nm. Recently, Toudert et al. [26] found that the absorption properties of spheroidal Bi nanoparticles were sensitive to its size, shape, and organization,

and also explored the tunability of the transverse resonance of Bi nanoparticles by controlling their size and shape. They predicted that “large” spheroidal Bi nanoparticles should be excellent candidates to obtain well-defined resonances that could be tuned from the near-UV to the near-infrared region. Fig. 5(b) shows that the as-prepared Bi metal particles were sphere-like with a diameter of around 1 μm . It is therefore reasonable to consider that high tunability of SPR from the UV through to the near-infrared region (beyond 800 nm) can be achieved by incorporation of Bi metal particles with a large size. The uniform dispersion of Bi spheres with average diameters of approximately 300 nm was well-coupled with the thick $g\text{-C}_3\text{N}_4$ layers (Fig. 5(c)). The decreased size of the Bi spheres in the Bi-CN composite compared with that of the Bi particles alone can be ascribed to a grain boundary size effect of $g\text{-C}_3\text{N}_4$ during the solvothermal thermal process. Because of the decreased size of Bi spheres in the composites, the SPR peak of Bi metal was not detected in Fig. 5(a). Gérard et al. [27] reported that the experimental scattering spectra of individual Al nanodisks with diameters varying from 70 to 180 nm displayed a bathochromic shift from around 300 to 550 nm as diameter increased. This provides evidence that the Bi-CN composites display an SPR peak (typically longer than 800 nm) originating from large Bi metal particles.

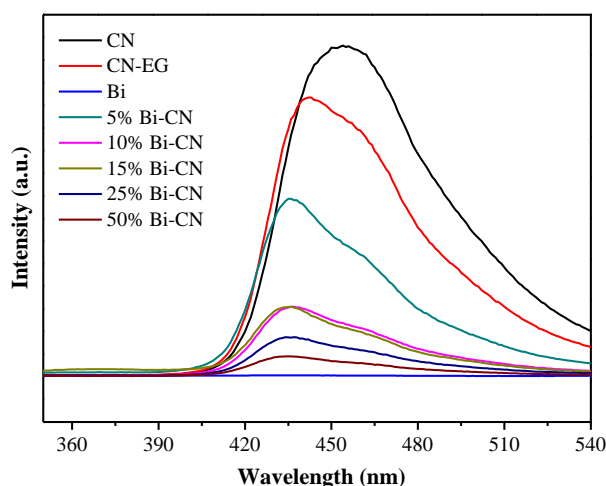


Fig. 6. PL spectra of $g\text{-C}_3\text{N}_4$ (CN), CN-EG, Bi, and Bi-CN composites.

Strong visible-light absorption is only one of the important factors to realize a high-efficiency photocatalytic composite. The effective separation of photogenerated electron-hole pairs in a photocatalytic composite is needed for efficient photo-oxidation of NO. Therefore, PL spectra of the composites were obtained, as shown in Fig. 6. After the addition of Bi metal, considerable PL quenching was observed for the Bi-CN composites. The obvious quenching of the PL emission peak intensity of the Bi-CN composites was attributed to unidirectional electron migration from the conduction band (CB) of $g\text{-C}_3\text{N}_4$ to Bi metal because of the Mott-Schottky effect of Bi metal [19]. Therefore, the Bi dispersed on the surface of $g\text{-C}_3\text{N}_4$ could effectively hinder electron-hole recombination, which is very promising for achieving photo-oxidation with satisfying activity. Aside from the different emission intensities of these photocatalysts, there are subtle yet revealing differences between these spectra. Compared with the peak for $g\text{-C}_3\text{N}_4$, those of both CN-EG and Bi-CN composites show a hypsochromic shift, which can be attributed to the quantum sizes effects originating from solvothermal treatment decreasing

the size of g-C₃N₄ layers, consistent with previous results [19].

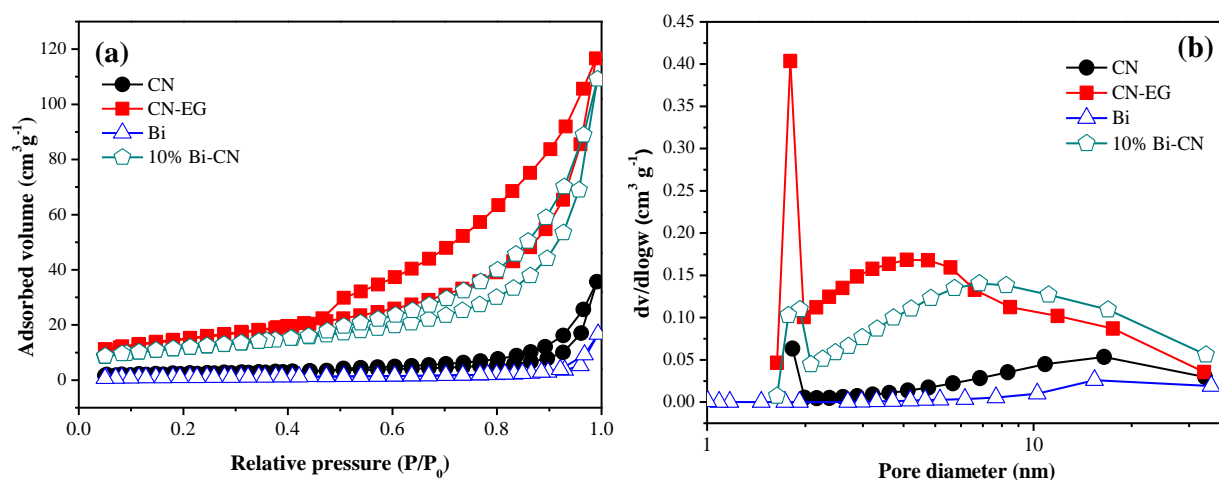
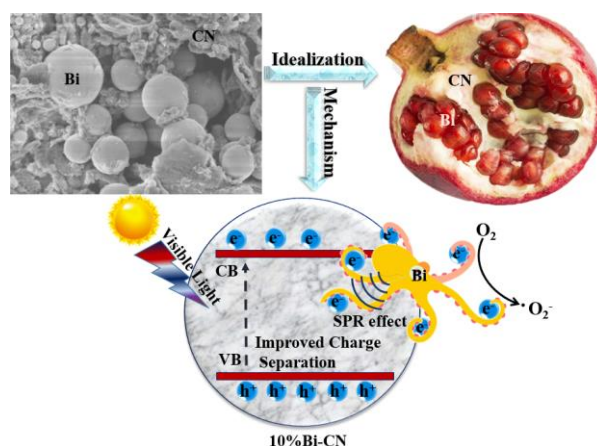


Fig. 7. Nitrogen adsorption–desorption isotherms (a), and the corresponding pore size distributions of the photocatalysts (b).

Specific surface area is another important parameter of photocatalysts. The specific surface area of each photocatalyst was determined by N₂ adsorption–desorption measurements to ascertain its possible contribution to photocatalytic reactions. Fig. 7(a) reveals that the isotherms were typical of type IV with a hysteresis loop observed at $P/P_0=0.5-1.0$. This suggests both g-C₃N₄ and the composites are mesoporous, with no evident plugging or change of the g-C₃N₄ structure after the inclusion of Bi metal (Table 1 and Fig. 7(b)). The specific surface area of CN-EG is 53 m² g⁻¹, which is about six times higher than that of pristine g-C₃N₄ (9 m² g⁻¹). The specific surface area of 10% Bi-CN is 42 m² g⁻¹, slightly lower than that of CN-EG. Additionally, the pore size distributions in Fig. 7(b) reveal that the pores in g-C₃N₄ and 10% Bi-CN are mainly distributed in the range of 1.8–6.8 nm, corresponding to mesoporous structure. Upon increasing the Bi content to 15%, the specific surface area and pore size distribution of the composite were almost unchanged but its photocatalytic activity deteriorated compared with that of the 10% Bi-CN composite. Consequently, this experiment ruled out the contribution of surface area to the photocatalytic activity of the composites.



Scheme 1. Proposed photocatalytic oxidation NO mechanism for the 10% Bi-CN composite.

From the perspective of maximizing the visible-light photocatalytic performance of the composites, we chose to elucidate a possible photocatalytic mechanism of the 10% Bi-CN composite. On the basis of the results described above, we propose

the following mechanism, as shown in Scheme 1. The appearance of the 10% Bi-CN composite with Bi spheres embedded in a g-C₃N₄ layer resembles pomegranate. The UV-vis DRS results indicated that the introduction of metallic Bi greatly enhanced the photoabsorption performance of the 10% Bi-CN composite because of the SPR effect of Bi metal. Meanwhile, the PL experiment revealed that the addition of Bi metal to g-C₃N₄ promoted the effective separation of photoexcited charge carriers because Bi metal in the composite formed a Schottky barrier at the metal/g-C₃N₄ interface [19]. These two factors are the basis of the high photoactivity of the 10% Bi-CN composite. Furthermore, the favorable coupling effect of Bi metal with g-C₃N₄ also plays an important role in its high photoactivity based on the results of photocatalytic testing. As illustrated in Scheme 1, the photogenerated electrons in the CB of g-C₃N₄ would transfer to metallic Bi because the CB of CN is more negative than the Fermi level of metallic Bi. Simultaneously, the holes accumulate in the VB of g-C₃N₄, which possesses sufficient oxidizing ability to degrade NO. This type of charge transmission greatly improved the separation of charge carriers and enabled the photogenerated electrons and holes to remain on the surface of metallic Bi and VB of g-C₃N₄, respectively, allowing them to react with air and water, and thus produce active species to realize photo-oxidation of NO.

3.4. Photocatalyst stability

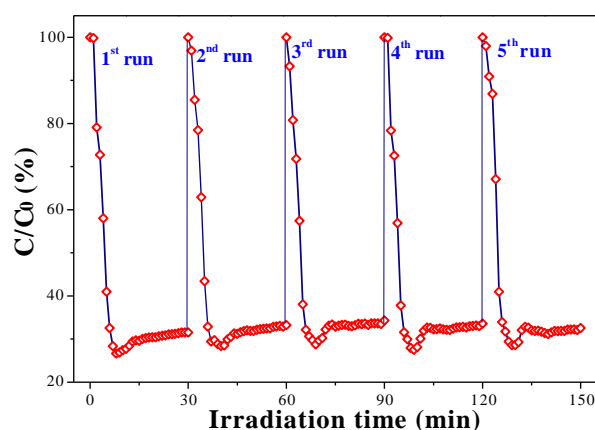


Fig. 8. Photocatalytic oxidation curves of NO reusing 10% Bi-CN.

It is known that photocorrosion might occur on the photocatalyst surface during photocatalytic reaction. To test the stability of the catalysts in NO photocatalytic oxidation, we reused the 10% Bi-CN photocatalyst five times. Fig. 8 shows that the activity of the photocatalyst after five cycles was nearly the same as that of the fresh one. The high stability of the photocatalyst was attributed to the strong interaction between pure Bi metal and g-C₃N₄, and indicates that composites consisting of g-C₃N₄ modified with pure Bi metal are promising for use in practical applications like air purification.

4. Conclusions

An in situ solvothermal treatment strategy to prepare Bi-CN composites with a pomegranate-like structure was developed. Pure Bi metal obtained using NaBiO₃·2H₂O as the precursor was successfully used to modify g-C₃N₄. Embedding pure spherical Bi metal particles in g-C₃N₄ layers had two main advantages. Firstly, because of the unique chemical and physical properties of pure Bi metal, together with the efficient function of the cocatalyst, the resulting Bi-CN composites displayed

strongly absorption light over the entire spectral range. Secondly, the favorable match of Bi with g-C₃N₄ resulted in beneficial Mott–Schottky effects at their interfaces, and thus a fast separation rate of photogenerated electrons and holes. The high stability of the obtained Bi-CN composites makes them promising for use in practical applications such as air purification.

Acknowledgement. This work was supported by the National Program on Key Basic Research Project (2016YFA0203000), the Early Career Scheme (ECS 809813) from the Research Grant Council, Hong Kong SAR Government, and the Croucher Foundation Visitorship for PRC Scholars 2015/16 at The Education University of Hong Kong. This work was also supported by the National Natural Science Foundation of China (51672312, 21373275) and the Program for New Century Excellent Talents in University (NCET-12-0668)

References:

- [1] Y.H. Li, L.P. Yang, G.H. Dong, W.K. Ho, *Molecules*, **2016**, 21, 36–46.
- [2] Q. Zhang, Y. Zhou, F. Wang, F. Dong, W. Li, H.M. Li, G.R. Patzke, *J. Mater. Chem. A*, **2014**, 2, 11065–11072.
- [3] P. Wan, B.B. Huang, Y. Dai, M.H. Whangbo, *Phys. Chem. Chem. Phys.*, **2012**, 14, 9813–9825.
- [4] M.A. El-Sayed, *Acc. Chem. Res.*, **2001**, 34, 257–264.
- [5] N. Pradhan, A. Pal, T. Pal, *Langmuir*, **2001**, 17, 1800–1802.
- [6] X.W. Liu, H.Q. Cao, J.F. Yin, *Nano Res.*, **2011**, 4, 470–482.
- [7] S.X. Weng, B.B. Chen, L.Y. Xie, Z.Y. Zheng, P. Liu, *J. Mater. Chem. A*, **2013**, 1, 3068–3075.
- [8] Y. Yu, C.Y. Cao, H. Liu, P. Li, F.F. Wei, Y. Jiang, W.G. Song, *J. Mater. Chem. A*, **2014**, 2, 1677–1681.
- [9] F. Dong, Q.Y. Li, Y.J. Sun, W.K. Ho, *ACS Catal.*, **2014**, 4, 4341–4350.
- [10] Z. Wang, C.L. Jiang, R. Huang, H. Peng, X.D. Tang, *J. Phys. Chem. C*, **2014**, 118, 1155–1160.
- [11] F. Dong, T. Xiong, Y.J. Sun, Z.W. Zhao, Y. Zhou, X. Feng, Z.B. Wu, *Chem. Commun.*, **2014**, 50, 10386–10389.
- [12] J. Zhang, T. He, B. Liu, L. Liu, Z.L. Zhao, D.Q. Hu, X.H. Ju, G.T. Wu, P. Chen, *Chin. J. Catal.*, **2013**, 34, 1303–1311.
- [13] Y. Shiraishi, S. Kanazawa, Y. Sugano, D. Tsukamoto, H. Sakamoto, S. Ichikawa, T. Hirai, *ACS Catal.*, **2014**, 4, 774–780.
- [14] P. Wang, S.H. Sun, X.Y. Zhang, X. Ge, W. Lü, *RSC Adv.*, **2016**, 6, 33589–33598.
- [15] X.C. Wang, K. Maeda, X.F. Chen, K. Takanabe, K. Domen, Y.D. Hou, X.Z. Fu, M. Antonietti, *J. Am. Chem. Soc.*, **2009**, 131, 1680–1681.
- [16] Y.J. Cui, *Chin. J. Catal.*, **2015**, 36, 372–379.
- [17] F. Dong, Z.L. Ni, P.D. Li, Z.B. Wu, *New J. Chem.*, **2015**, 39, 4737–4744.
- [18] B. Yuan, J.X. Wei, T.J. Hu, H.B. Yao, Z.H. Jiang, Z.W. Fang, Z.Y. Chu, *Chin. J. Catal.*, **2015**, 36, 1009–1016.
- [19] F. Dong, Z.W. Zhao, Y.J. Sun, Y.X. Zhang, S. Yan, Z.B. Wu, *Environ. Sci. Technol.*, **2015**, 49, 12432–12440.

- [20] Q.L. Gu, K.J. Zhu, N.S. Zhang, Q.M. Sun, P.C. Liu, J.S. Liu, J. Wang, Z.S. Li, *J. Phys. Chem. C*, **2015**, 119, 25956–25964.
- [21] Y.H. Li, Y.J. Sun, F. Dong, W.K. Ho, *J. Colloid Interface Sci.*, **2014**, 436, 29–36.
- [22] T. Xiong, W.L. Cen, Y.X. Zhang, F. Dong, *ACS Catal.*, **2016**, 6, 2462–2472.
- [23] Y.J. Sun, T. Xiong, Z.L. Ni, J. Liu, F. Dong, W. Zhang, W.K. Ho, *Appl. Surf. Sci.*, **2015**, 358: 356–362.
- [24] E.R. Swy, A.S. Schwartz-Duval, D.D. Shuboni, M.T. Latourette, C.L. Mallet, M. Parys, D.P. Cormode, E.M. Shapiro, *Nanoscale*, **2014**, 6: 13104–13112.
- [25] Y. Wang, J. Yao, H.R. Li, D.S. Su, M. Antoniet, *J. Am. Chem. Soc.*, **2011**, 133: 2362–2365.
- [26] J. Toudert, R. Serna, M.J. de Castro, *J. Phys. Chem. C*, **2012**, 116: 20530–20539.
- [27] D. Gérard, S.K. Gray, *J. Phys. D: Appl. Phys.*, **2015**, 48: 1–14.

Enhanced visible-light photo-oxidation of nitric oxide using bismuth-coupled graphitic carbon nitride composite heterostructures

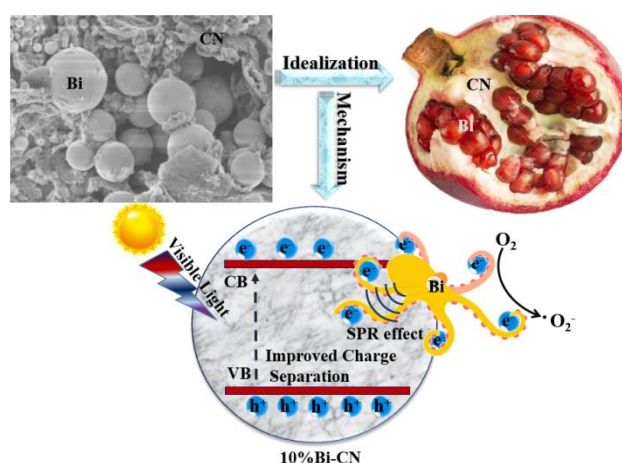
LI Yuhan^a, LV Kangle^{a,c,*}, HO Wingkei^{a, b*}, ZHAO Zaiwang^a, HUANG Yu^b

^aDepartment of Science and Environmental Studies, The Education University of Hong Kong, Tai Po, N.T., Hong Kong, China

^bKey Laboratory of Aerosol Chemistry and Physics, Institute of Earth Environment, Chinese Academy of Sciences, Xi'an 710061, Shanxi, China

^cKey Laboratory of Catalysis and Materials Science of the State Ethnic Affairs Commission and Ministry of Education, College of Resources and Environmental Science, South-Central University for Nationalities, Wuhan 430074, Hubei, China

The introduction of bismuth metal to graphitic carbon nitride resulted in composites that displayed improved light absorption over the entire visible range, effective separation of photogenerated electron–hole pairs, and high visible-light photocatalytic activity in oxidation of NO.



石榴状单质铋(Bi)球与 $g-C_3N_4$ 复合材料表现出超强可见光氧化 NO 性能

李宇涵^a, 吕康乐^{a,c,*}, 何咏基^{a,b,*}, 赵再望^a, 黄宇^b

^a 香港教育大学 科学与环境系, 香港

^b 中国科学院地球环境研究所 气溶胶化学与物理重点实验室, 陕西西安 710061

^c 中南民族大学 资源与环境学院, 湖北武汉 430074

摘要: 采用一种原位合成工艺制备了具有类石榴结构的金属铋(Bi)单质修饰的 $g-C_3N_4$ 复合材料(Bi-CN), 并用于可见光氧化 NO 反应中。金属铋(Bi)单质镶嵌在 CN 层间形成的复合物, 由于金属铋单质显著的表面等离子体共振(SPR)作用可将光吸收范围由紫外光延展至近红外, 极大地提高了复合物的光吸收。此外, 由于金属铋单质存在于复合物界面可产生内建莫特-肖特基效应, 从而加快光生载流子的分离与转移。由此, Bi-CN 复合物光催化剂展现出超强的光催化去除 NO 性能。我们提出了类石榴结构的形成以及相应的 Bi-CN 复合物光催化活性的提高机理。这不仅为高效的金属铋单质改性的 $g-C_3N_4$ 基光催化剂提供了一种新的设计方案, 也对 $g-C_3N_4$ 基光催化的机制理解提出了新的见解。

通过 X 射线衍射、红外光谱和 X 射线光电子能谱结果发现铋是以金属单质的形式存在于 Bi-CN 复合物中, 这得益于我们采用了二水合铋酸钠($NaBiO_3 \cdot 2H_2O$)作为铋前驱体, 从而成功避免了氧化态铋的形成。Bi-CN 复合物中金属铋单质的存在有诸多优点。首先, 金属铋单质具有显著的表面等离子体共振效应(SPR), 它的引入可大大提高复合物的光吸收能力和太阳光利用率。有研究表明, 直径为 150-200 nm 的铋球能够在紫外-可见漫反射图谱(UV-vis)在 $\lambda=500$ nm 处呈现出典型的 SPR 峰, 但本样品在 $\lambda=200-800$ nm 区间内并未发现该 SPR 峰。由于铋单质的共振受限于其尺寸大小、颗粒形状和构造环境。本文中球形铋单质的直径约为 1 μm , 其可能发生共振效应的峰位置应超过 800 nm, 由而未发现相应的 SPR 峰。其次, 金属铋单质分散在 CN 层表面上构建的肖特基势垒能够高效地阻止光生电子与空穴的复合, 促进了光生载流子的分离与转移, 从而提高光氧化 NO 进程。再者, 金属铋单质的介入成功构造了 Bi-CN 异质结, 在可见光照射下 NO 氧化反应中, Bi-CN 复合物活性显著高于 CN (22.2%)、CN-EG (36.4%) 和 Bi (14.1%), 其中以 10% Bi-CN 活性最佳, NO 去除率到 70.4%, 远远超过 K 插层的 $g-C_3N_4$ 、Ag 掺杂的 $g-C_3N_4$ 和氧化石墨烯修饰的 $g-C_3N_4$ 。

然而, 当复合物中金属铋单质含量超过 10%时, 其活性明显下降。这是因为大量的金属铋单质积聚在 Bi-CN 复合物表面上而造成物理堵塞, 妨碍了 CN 吸收可见光, 从而降低了其可见光吸收能力; 同时导致只会吸收更多的紫外光 ($\lambda < 280$ nm) 而不是可见光, 因而其可见光催化氧化 NO 能力下降。

关键词: 金属铋; 表面等离子体共振; 光氧化; 一氧化氮; 可见光; 石墨型碳化氮

收稿日期: 2016-08-30.接受日期: 2016-10-5.出版日期: 2016-.

*通讯联系人. 电话: (852)29488255; 传真: (852) 29487726;

电子信箱: lvkangle@mail.scuec.edu.cn(K.L. Lv);

*通讯联系人. 电子信箱: keithho@ied.edu.hk (W.K. Ho)

This is the pre-published version.

基金来源: 国家自然科学基金(51672312, 21373275); 新世纪优秀人才支持计划 (NCET-12-0668) .

本文的英文电子版由 Elsevier 出版社在 ScienceDirect....